Lattice Metamaterials with Mechanically Tunable Poisson's Ratio for Vibration Control

Yanyu Chen,[1] Tiantian Li,[1] Fabrizio Scarpa,[2] and Lifeng Wang[1,*]
[1]*Department of Mechanical Engineering, State University of New York at Stony Brook, Stony Brook, New York 11794, USA*
[2]*Advanced Composites Centre for Innovation and Science, University of Bristol, Bristol BS8 1TR, United Kingdom*
(Received 29 September 2016; revised manuscript received 20 December 2016; published 9 February 2017)

Metamaterials with artificially designed architectures are increasingly considered as new paradigmatic material systems with unusual physical properties. Here, we report a class of architected lattice metamaterials with mechanically tunable negative Poisson's ratios and vibration-mitigation capability. The proposed lattice metamaterials are built by replacing regular straight beams with sinusoidally shaped ones, which are highly stretchable under uniaxial tension. Our experimental and numerical results indicate that the proposed lattices exhibit extreme Poisson's-ratio variations between −0.7 and 0.5 over large tensile deformations up to 50%. This large variation of Poisson's-ratio values is attributed to the deformation pattern switching from bending to stretching within the sinusoidally shaped beams. The interplay between the multiscale (ligament and cell) architecture and wave propagation also enables remarkable broadband vibration-mitigation capability of the lattice metamaterials, which can be dynamically tuned by an external mechanical stimulus. The material design strategy provides insights into the development of classes of architected metamaterials with potential applications including energy absorption, tunable acoustics, vibration control, responsive devices, soft robotics, and stretchable electronics.

DOI: 10.1103/PhysRevApplied.7.024012

I. INTRODUCTION

Metamaterials are rationally designed multiscale material systems whose unusual equivalent physical properties are dictated by their architectures rather than compositions. Metamaterials have recently attracted significant interest within the research community because of their intrinsic capability of exhibiting unusual properties for broad ranges of potential applications [1–3]. For example, metamaterials with artificially designed architectures can exhibit a negative refractive index that is unattainable for conventional materials [4–6]. The metamaterial concept has been rapidly extended from photonic systems to acoustic [7–10] and mechanical systems [11–16]. Among them, the mechanical metamaterials with a negative Poisson's ratio (NPR) are of particular interest [17–26]. For instance, by tailoring the geometric features of the ligaments in cellular structures, auxetic behavior can be achieved over a wide range of geometric parameters [24,25]. In addition, by integrating topology optimization with a 3D printing technique, architected materials with nonstraight ligaments have been optimized and display a nearly constant Poisson's ratio over large deformations [26]. Most materials (both isotropic and anisotropic) exhibit positive Poisson's ratios (PPRs), however, the existence of negative Poisson's ratios is still permitted under the tenets of the classic theory of elasticity.

Materials with a negative Poisson's ratio that will contract (expand) transversally when they are axially compressed (stretched) are also called auxetics [27–35]. Auxetic behavior has been observed in a variety of natural systems, including cubic metals [36], zeolites [37,38], natural layered ceramics [39], silicon dioxides [40], single-layer graphene [41,42], and 2D protein crystals [43]. Following the seminal work of Lakes [30], a significant body of research work has been established to develop materials with a negative Poisson's ratio. For example, the auxetic behavior of materials provides a wrapping effect around a penetrating object when subjected to indentation, a feature that may be useful in protective and blast engineering applications [44–46]. Several microstructure architectures and deformation mechanisms have been developed to obtain the auxetic behavior. Between the various architectures it is worthwhile to note dimpled and perforated elastic sheets [47], origami-Kirigami-based metamaterials [18,48,49], hierarchical metamaterials with fractal cuts [50], and foams [51–55]. Auxetic materials and structures are intrinsically multifunctional because of the coupling originating between their unusual deformation mechanisms and their multiphysics behavior. For example, piezoresistive sensors with an auxetic substrate demonstrate a 300% improvement in piezoresistive sensitivity, making them capable of multimodal sensing [55].

Most of the theoretical and experimental investigations related to auxetic cellular materials are focused on

*Corresponding author.
Lifeng.wang@stonybrook.edu

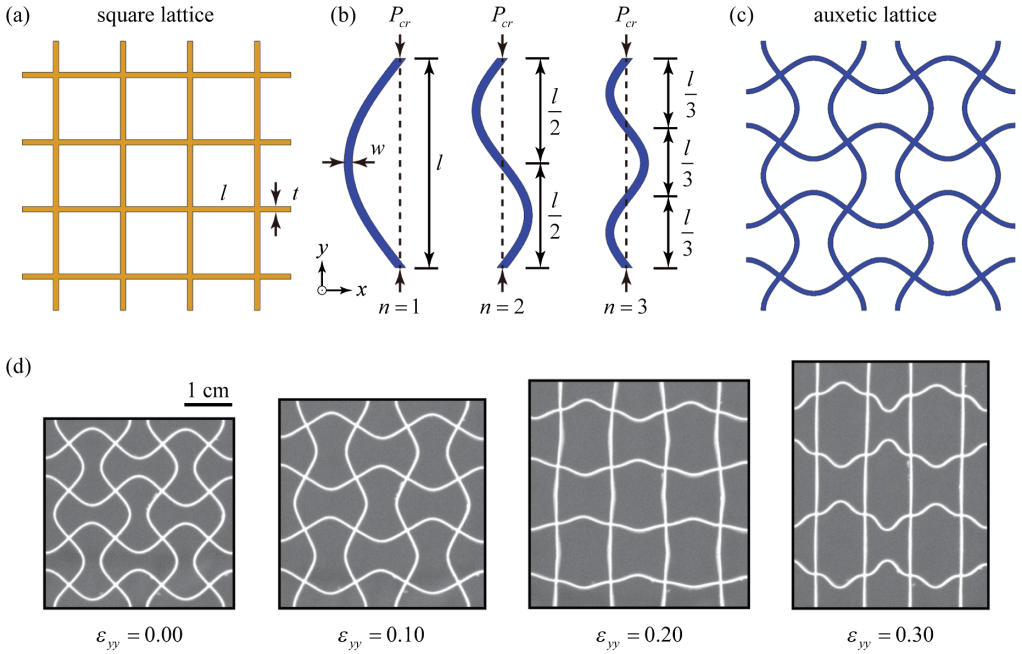

FIG. 1. Schematics and deformation behavior of the sinusoidally architected lattice material. (a) Regular square lattice with 2×2 unit cells. Here, t and l are the width and length of regular beams. (b) Buckling modes of a single beam under compression. (c) Proposed architected lattice metamaterials with 2×2 unit cells with $n = 1$. (d) Deformation behavior of the center area consisting of 2×2 unit cells of the architected lattice material under uniaxial tension.

microstructure configurations with straight ligament topologies. Recent numerical and experimental studies indicate that thin film materials with serpentine microstructures can have improved stretchability, owing to the introduced microstructure and small intrinsic strain in the materials [56–59]. A nonstraight (corrugated) rib configuration for open-cell polyurethane foams has also recently been considered as a likely explanation for the existence of an unusual blocked-shape memory effect in auxetic open-cell polyurethane foams [60]. Although it has been theoretically shown that the auxetic behavior can also be attained in hierarchically architected lattice metamaterials with triangular topology [57], convincing experimental evidence of the auxetic behavior of these materials has not been reported yet. Moreover, little attention has been paid to the performance of engineered auxetic metamaterial lattices with sinusoidally curved (nonstraight) ligaments in their microstructure, especially at the hierarchical level. The goal of this work is to investigate the auxetic behavior and vibration-control capability of one of these materials by combining computational modeling with 3D printing techniques and related experimental testing.

Here, we create the architected lattice metamaterials by replacing the regular straight beams with beams of sinusoidal shape (Fig. 1). Our metamaterial design concept is motivated by the observation that conventional lattice metamaterials have small or no wave band gaps [61,62], while tunable phononic band gaps could arise in buckled structures [63]. In addition, buckled or curved beams have an excellent stretchability under tension because the local strain is much smaller than the macroscopic strain when the lattice metamaterials are subjected to uniaxial stretch. Note that here we are not able to create the desired buckled-lattice metamaterials using external mechanical loading, because the short-wavelength buckling mode is never preferred for regular lattice metamaterials under macroscopic compression. We numerically and experimentally investigate the macroscopic auxetic response of the proposed lattice metamaterials over large strains of up to 50% in tension. Our results indicate that the Poisson's ratios can be effectively tuned from negative to positive, which is attributed to the deformation behavior of sinusoidally curved beams transiting from bending-dominated to stretching-dominated behavior. We further show that by tailoring the amplitude and wavelength of the sinusoidally curved beams it is possible to efficiently control this transition phenomenon. The proposed lattice metamaterials exhibit significant broad phononic band gaps when compared with regular square-lattice metamaterials. In particular, these band gaps can be dynamically tuned by applying an external mechanical stimulus, such as uniaxial stretching in our case.

II. DESIGN AND FABRICATION OF METAMATERIALS

A schematic of our 2D lattice microstructure with auxetic behavior is illustrated in Figs. 1(a)–1(c). The shape of the sinusoidally curved beams can be mathematically described as $y = A_n \sin(n\pi x/l)$, where A_n is the wave amplitude, n is the number of half wavelengths, and l is the length of regular straight beams. The length of the sinusoidally curved beam is given by

$$s = \int_0^l \sqrt{1 + (y')^2}\,dx = \int_0^l \sqrt{1 + \left[\frac{A_n n\pi}{l}\cos\left(\frac{n\pi x}{l}\right)\right]^2}\,dx. \quad (1)$$

Under the mass equivalence assumption, the width of the sinusoidally curved beam can be calculated as

$$w = tl \Big/ \int_0^l \sqrt{1 + \left[\frac{A_n n\pi}{l}\cos\left(\frac{n\pi x}{l}\right)\right]^2}\, dx, \qquad (2)$$

where t is the width of regular beams. Then, for a given $A_n n/l$, the width of the sinusoidally curved beam is the same for any n. In this work, we focus on structures with a volume fraction smaller than 0.1, where $l/t > 15$ for all cases.

The proposed lattice metamaterials are fabricated using a multimaterial 3D printer (Objet Connex260, Stratasys). To ensure the stretchability of the cellular configuration, a rubberlike material, FLX9795-DM, is used as the constitutive (core) material for the sinusoidally shaped beams [64]. Figure 1(d) shows the center area of the specimen, which consists of an array of 4×5 unit cells with $A_n n/l = 1/3$, $n = 1$, $w/l = 1/20$, and a representative sequence of images taken at different tensile strains. By simple inspection it is evident that at a small initial strain the lattice material expands transversally, indicating, therefore, the presence of an auxetic behavior. However, when the macroscopic tensile strain increases to 30%, the lattice material starts to contract along the x direction. These phenomena suggest that the fabricated 2D lattice metamaterials exhibit auxetic behavior and a strain-dependent Poisson's ratio.

To understand from a quantitative point of view the auxetic behavior of the square-lattice metamaterials, we have fabricated and mechanically tested three specimens consisting of 4×5 unit cells, where $A_n n/l = 1/3$ and $n = 1$, 2, 3, respectively [64]. To verify our design, numerical simulations are also performed on each specimen topology by using a nonlinear finite element code (COMSOL Multiphysics). The rubberlike constitutive material is modeled using the Arruda-Boyce hyperelastic model [65]. In addition, plane strain conditions are assumed in the simulation and the out-of-the-plane thickness of the 2D lattices is 1 cm [64].

III. MECHANICALLY TUNABLE POISSON'S RATIO

A. Auxetic behavior of lattice metamaterials

Figure 2(a) shows the macroscopic stress-strain relations of three selected specimens under uniaxial tension. The Arruda-Boyce hyperelastic model can accurately capture the mechanical behavior of the lattice metamaterials. At a high strain level, numerical predictions slightly deviate from the experimental measured data. The discrepancy between numerical and experimental data is mainly due to the failure of some beam ligaments. When the applied strain is higher than 0.35, some beams start to break, leading to the drop in the stress-strain curves. Since the specimens are fabricated layer by layer in the 3D printer, anisotropy, porosity, and imperfections are introduced during 3D printing [66,67], also playing a role. These specific aspects are not taken into consideration in our model.

We find that these structures exhibit J-shaped stress-strain curves, which are very similar to the mechanical response of bioinspired soft-network composite materials and other stretchable electronics [56–59]. However, the stress-strain behavior is different from that of plates with rectangular auxetic perforations, which exhibit a softening phenomenon in the tensile stress-strain curve for an increasing magnitude of Poisson's ratio [44]. Apparently, at small strains the structure has an auxetic behavior, moving from a more antirubber behavior ($n = 1$) to be marginally auxetic ($n = 3$, $\nu_{yx} \sim 0$). The lowest stiffness at small and medium strains (up to ~0.20) belongs to the specimens with the most negative ν_{xy}. That means that under tensile loading the cross section of the specimen increases, and therefore for a given tensile force the equivalent stress is lower. Close to a critical strain (i.e., when $\nu_{yx} \sim 0$), the lattice tends to provide an equivalent constant cross section for increasing strains. Densification is apparent at strains close to 0.22–0.25, when the Poisson's ratio tends to change dramatically and decreases its magnitude, coming close to being marginally auxetic or even a slightly PPR, depending on the sinusoidal order adopted. This unique deformation behavior is intrinsically dictated by the sinusoidal architecture of the artificially designed ligaments. The preset configuration of the sinusoidally shaped ligaments enables switching deformation mechanisms between bending and stretching of the ligaments [68]. In conventional lattice materials with straight beams this deformation transformation is not envisioned.

The numerical and experimental results of the Poisson's ratio of the lattice metamaterials as a function of the tensile strain are presented in Fig. 2(b). For tensile strains below 0.20, the numerical predictions tend to slightly overestimate the experimental results for $n = 1$ and 2. Note that since the lattice metamaterials are soft, unavoidable misalignments in the test setup can influence the measurement of the Poisson's ratios. Furthermore, when calculating the Poisson's ratio by means of digital image correlation, minor errors can be introduced in the processing. We also note that over this range of strain, the proposed square-lattice metamaterials exhibit a nearly constant negative Poisson's ratio. This is because vertical and horizontal beams are both subjected to bending at macroscopic strains below 0.2 [Fig. 2(c)]. At this small strain range, the magnitudes of the vertical and horizontal strain increments are changing in a similar manner. As a result, the Poisson ratio is nearly constant. With the increase of the stretching, the Poisson's ratio gradually turns from negative to marginally positive. To elucidate the mechanisms responsible for the transition of the Poisson's ratio, we present the mechanical response of a representative unit cell taken from the central area of

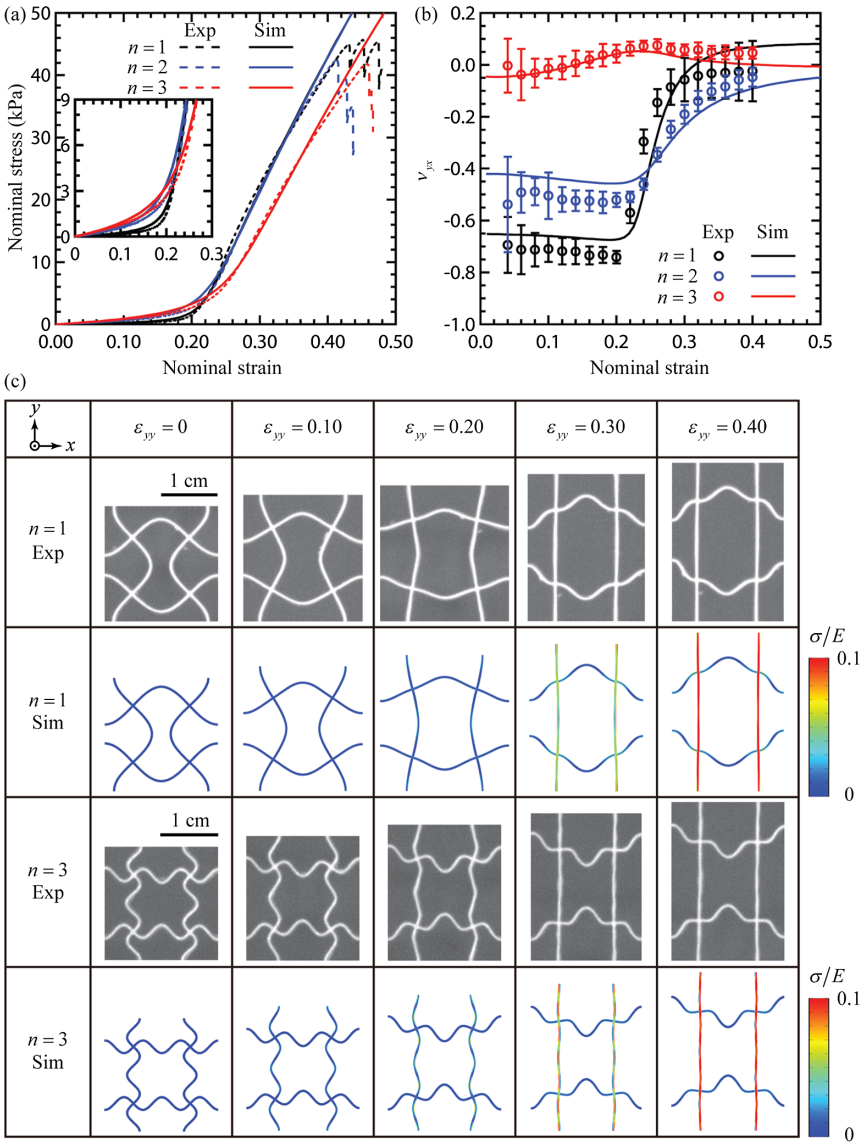

FIG. 2. (a) Stress-strain relations of the architected lattice metamaterials. (b) Evolution of the Poisson's ratios as a function of the applied tensile strain. (c) Deformed configuration at different macroscopic strains. The von Mises stresses are normalized with respect to the Young's modulus of the constitutive materials. Here, $A_n n/l = 1/3$.

the specimen under different tensile strains [Fig. 2(c)]. Here, we show only the mechanical behavior of the lattice metamaterials with $n = 1$ and 3. Again, one can notice an excellent agreement between the numerical and the experimental deformations. At strains below ~0.20, the deformation response of the vertical beams is clearly bending dominated due to the initial curvature of sinusoidal architecture. With the increase of macroscopic stretching, the sinusoidal architecture will be stretched to an approximately straight beam. As a result, the deformation behavior will become stretching dominated and very similar to regular materials, which typically exhibit a positive or zero Poisson's ratio. Here, the numerical and experimental results demonstrate that a mechanically tunable negative Poisson's ratio can be achieved by introducing curved sinusoidal beams in regular lattice structures. The evolution of the Poisson's ratio strongly depends on the coupled deformation behavior of vertical and horizontal beams.

B. Mechanically tunable Poisson's ratios

Having demonstrated that the sinusoidally architected lattice metamaterials exhibit auxetic behavior under uniaxial tension at specific strain ranges, we now systematically investigate the effects of amplitude $A_n n/l$ and half wavelength n on the mechanical response and the Poisson's ratios. Figure 3(a) shows the stress-strain relations of the lattice metamaterials with different $A_n n/l$ and n. Each structure exhibits a J -shaped stress-strain curve, which is similar to our previous experimental observation. For a given amplitude, a short wavelength (i.e., a large n) gives rise to a higher stress-strain curve, indicating the presence of a significantly stiffer mechanical response. For a given value of n a smaller wave amplitude (i.e., a smaller curvature but with a larger beam width), however, leads to a higher stress-strain curve within the small strains range. These mechanical responses are intrinsically controlled by the bending stiffness of the sinusoidal curved beams, which

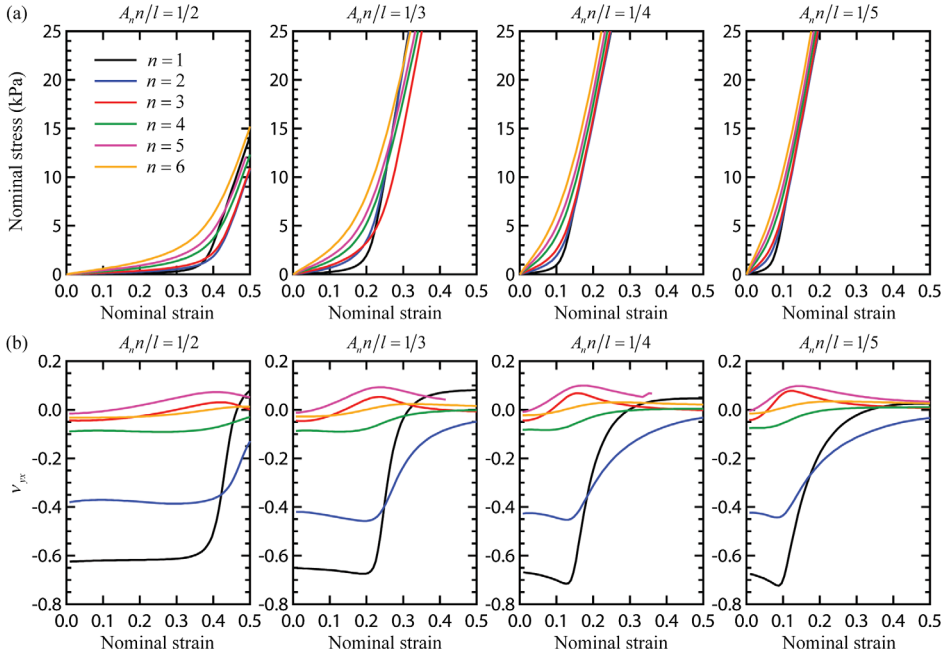

FIG. 3. Effect of (a) amplitude $A_n n/l$ and (b) number of half wavelength n on the stress-strain relation and Poisson' ratio. Here, $w/l = 1/20$ for all of the simulations.

is defined as $S = CE\kappa w^3$, where C is the geometric constant, E is the Young's modulus of the beam, κ is the curvature, and w is the width of the beam. The effective stiffness of the lattice metamaterials as a function of $A_n n/l$ and n is summarized in Fig. 4(a). We further note that for a given wave amplitude a significant auxetic behavior can be observed for $n = 1$, 2 [Fig. 3(b)]. Interestingly, the transition strain for the in-plane Poisson's ratio is proportional to the wave amplitude because large macroscopic stretching is needed to make straight vertical beams with larger wave amplitudes. The minimum Poisson's ratios as a function of $A_n n/l$ and n are summarized in Fig. 4(b).

We have numerically demonstrated that the geometric parameters of the sinusoidally curved beams have a great impact on the evolution of the Poisson's ratio. Among these, the number of half wavelength n is critical to the existence of the auxetic behavior. For a smaller n, strong synergistic deformation behavior exists between horizontal behavior and vertical behavior. As a result, the preexisting deformation can be harnessed to generate an auxetic behavior. However, with the increase of n, this synergistic deformation between vertical and horizontal beams becomes weak. For a given n, the wave amplitude is crucial to the transition between the negative Poisson's ratio and the positive Poisson's ratio.

Another geometric parameter with a significant impact on the mechanical response and in-plane Poisson's ratios is the slenderness ratio w/l. To demonstrate this, we examine the mechanical response and the auxetic behavior of the lattice material with $A_n n/l = 1/3$ and $n = 1$, 2. Highly nonlinear stress-strain curves arise in those cases for a small strain range [Fig. 5(a)] because the mechanical response of the sinusoidally curved beam is bending dominated, with the bending stiffness being proportional to w^3. Therefore, the large slenderness ratio will give rise to a higher stiffness. At large strains, the mechanical response of the sinusoidally curved beam becomes stretching dominated and a nearly linear response can be observed in the stress-strain curves.

The bending-dominated and stretching-dominated behaviors at different strains have also a significant impact on the Poisson's ratios [Fig. 5(b)]. At strains below 0.20, the lattice metamaterials with $n = 1$ and 2 have a nearly constant negative Poisson's ratio of ~ -0.65 and ~ -0.45, respectively. This phenomenon indicates that the Poisson's ratio is almost independent of the slenderness ratio when the

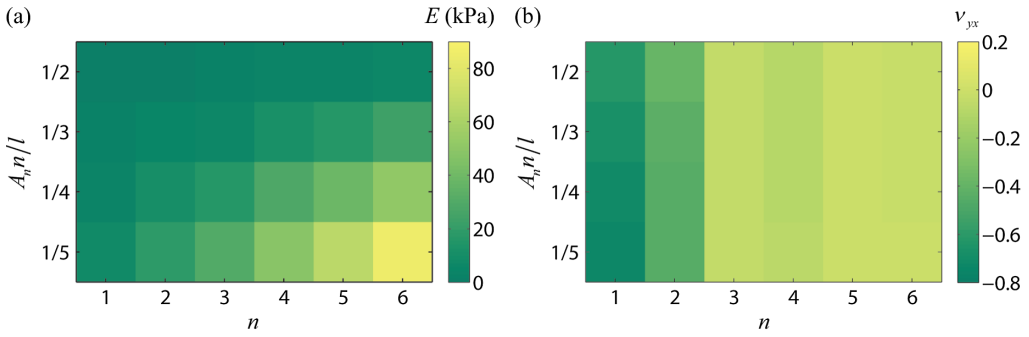

FIG. 4. Effect of amplitude $A_n n/l$ and the number of half wavelength n on the (a) effective stiffness and (b) Poisson' ratio of the proposed lattice metamaterials.

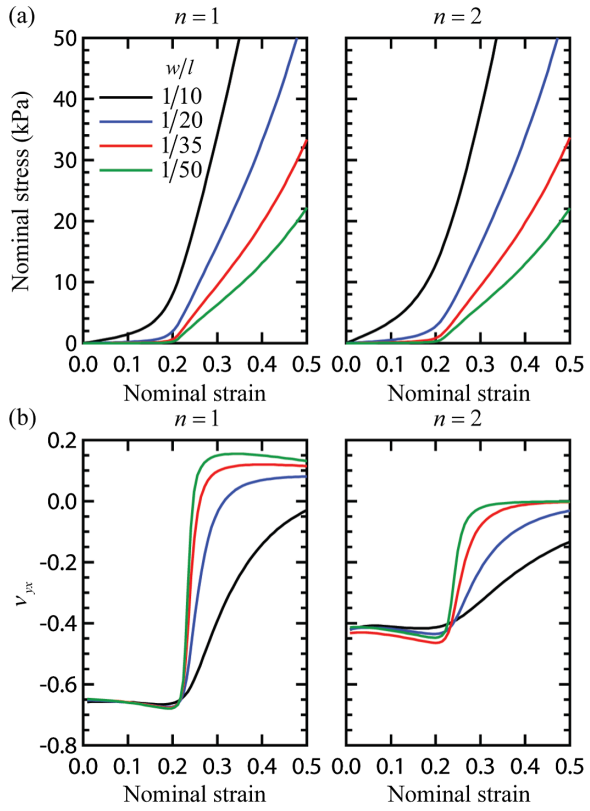

FIG. 5. Effect of w/l on (a) the stress-strain relation and (b) Poisson's ratios of the lattice metamaterials. Here, $A_n n/l = 1/3$.

sinusoidally curved beams are highly bending dominated. By contrast, at large stretching strain, the Poisson's ratio rapidly changes from negative to positive for both cases. The transition is much sharper for a smaller slenderness ratio, since the nearly straight beam is, in this case, more compliant.

C. Effect of the lattice topology

Having shown that the mechanical response and the Poisson's ratios can be tuned by tailoring the geometric features of the sinusoidally curved beams, we now proceed to examine the effect of the lattice topology on the auxetic behavior from a numerical and an experimental standpoint. Four types of sinusoidally architected lattice metamaterials with hexagonal, Kagome, square, and triangular topology are fabricated using 3D printing [Fig. 6(a)]. Here, we use as geometry parameters $A_n n/l = 1/3$ and $n = 2$. The specific lattice topology has a significant impact on the overall mechanical response of the lattice metamaterials under tension [Fig. 6(b)]. The triangular lattice has (as expected) the largest stiffness, while the hexagonal tessellation is the more compliant [69]. Experimental and numerical results related to the Poisson's ratios for the four types of topology are presented in Fig. 6(c), and they all show a good agreement. In contrast to the negative Poisson's ratio of square-lattice metamaterials, both hexagonal and kagome lattice configurations exhibit a positive Poisson's ratio below 0.40 tensile strains. The evolution of the Poisson's ratio of the triangular lattice is, however, strongly strain dependent, and there is a switch between NPR and PPR at a critical strain of 24%.

This metamaterial design concept can be extended to other lattice topologies, thereby offering different deformation behaviors and mechanical responses. For example, it is well known that regular beams in hexagonal lattices are bending dominated, while the introduction of sinusoidally curved beams enables the coexisting of bending and stretching behavior. The study of the effect of lattice topology not only provides opportunities to tailor the auxetic behavior, but also provides us a better understanding of the coupling deformation behavior in novel

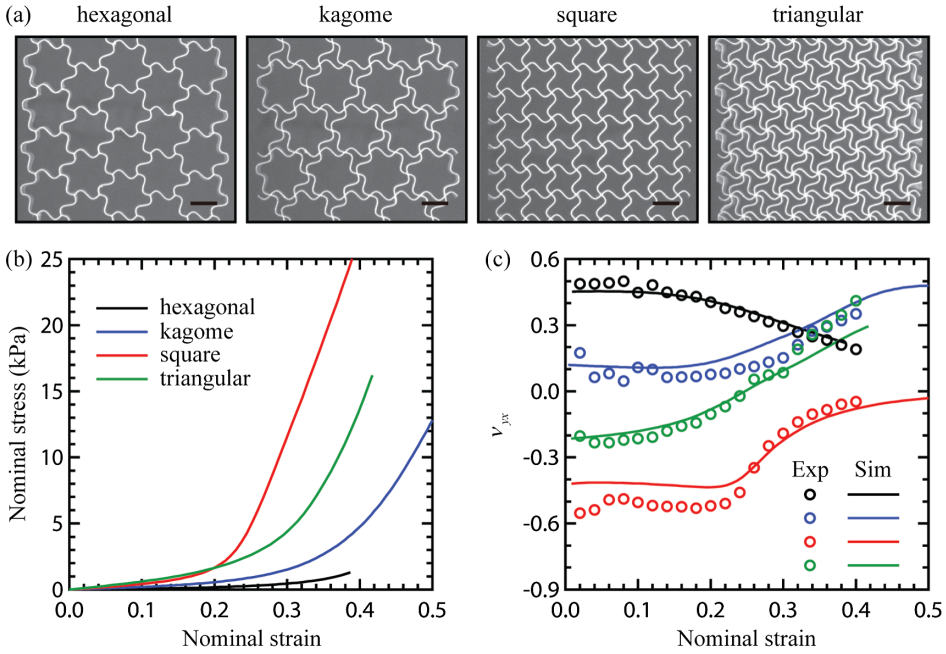

FIG. 6. Effect of the topology on the stress-strain curves and Poisson's ratio. (a) 3D printed specimens with hexagonal, kagome, square, and triangular topology. (b) Stress-strain relations and (c) evolution of Poisson's ratio as a function of the strain. The legend is the same as that in (b). Here, $A_n n/l = 1/3$, $n = 2$, and $w/l = 1/20$. Scale bar: 1 cm.

lattice metamaterials. It is anticipated that topologies, along with sinusoidal architecture, can be used to explore mechanical properties and other functionalities.

IV. BROADBAND AND MECHANICALLY TUNABLE VIBRATION MITIGATION

A. Broad and multiple phononic band gaps

We have demonstrated that the proposed sinusoidally architected lattice metamaterials exhibit tunable Poisson's ratios over a large tensile strain range. The evolution of Poisson's ratio strongly depends on the geometric features of the sinusoidal architecture as well as the global topology of the lattice metamaterials. From a metamaterial design perspective, the interplay between Poisson's ratios and the intrinsic architecture can guide us to explore other functionalities arising from the use of these architected materials. In this section, we investigate the elastic wave propagation occurring within these lattice metamaterials and explore their capability in providing a dynamic tunability for vibration alleviation using an external mechanical stimulus.

We start by examining the phononic dispersion relations and the transmission spectra of the lattice metamaterials [64,70–74]. In our case, the normalized frequency is defined as $\Omega = \omega/\omega_1$, where ω is the frequency of the elastic wave obtained by solving the Bloch eigenvalue problem and $\omega_1 = \pi^2\sqrt{Et^2/12\rho l^4}$ is the first pinned-pinned flexural resonance frequency of a lattice beam [61]. For the material and structures studied in this work, $\omega_1 = 982$ Hz.

Figures 7(a)–7(d) show the phononic dispersion relations and the associated transmission spectra of a regular lattice material ($A = 0$, $n = 0$) and configurations with $A_n n/l = 1/3$ and $n = 1$, 3, 5. The simulated transmission spectrum for each lattice material agrees extremely well with the presence of the partial band gaps along the M-K direction found via the Bloch wave analysis. No band gaps exist in the regular lattice material, however, five complete band gaps can be observed for the sinusoidally architected lattice material with $n = 1$. Within the observed band gaps, the largest one lies within $\Omega = 1.12$–1.36. Both multiple and broad phononic band gaps arise for $n = 3$ and 5. More specifically, five and six complete band gaps emerge for $n = 3$ and 5, and the maximum band gaps for $n = 3$ and 5 lie within $\Omega = 3.25$–3.59 and $\Omega = 0.79$–1.26, respectively. A direct comparison between the geometric features of the regular and proposed lattice metamaterials shows that mechanisms associated with the broad and multiple band-gap formation are intrinsically dictated by the wave amplitude and wavelength of the sinusoidally curved beams, leading to the coupling of axial and bending motion [75]. The formation of complete wave-band gaps can be

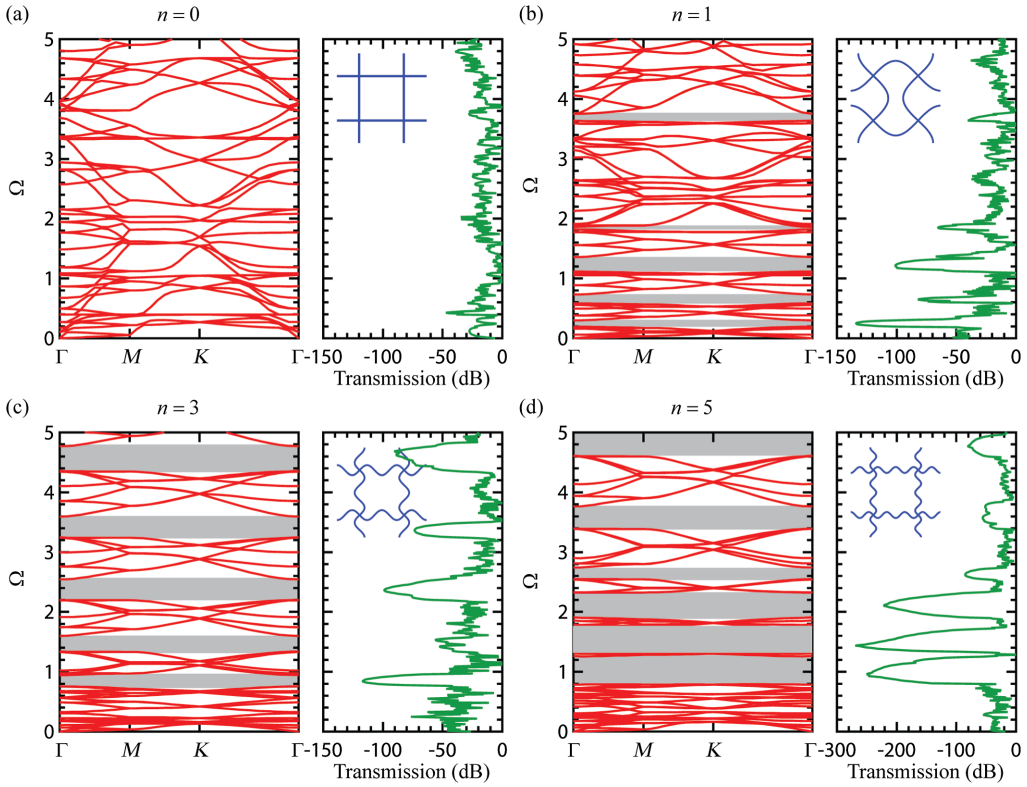

FIG. 7. Phononic dispersion relations and transmission spectra of the architected lattice metamaterials. (a) $A = 0$, $n = 0$; (b) $A_n n/l = 1/3$, $n = 1$; (c) $A_n n/l = 1/3$, $n = 3$; (d) $A_n n/l = 1/3$, $n = 5$. Here, $w/l = 1/20$ for all of the simulations.

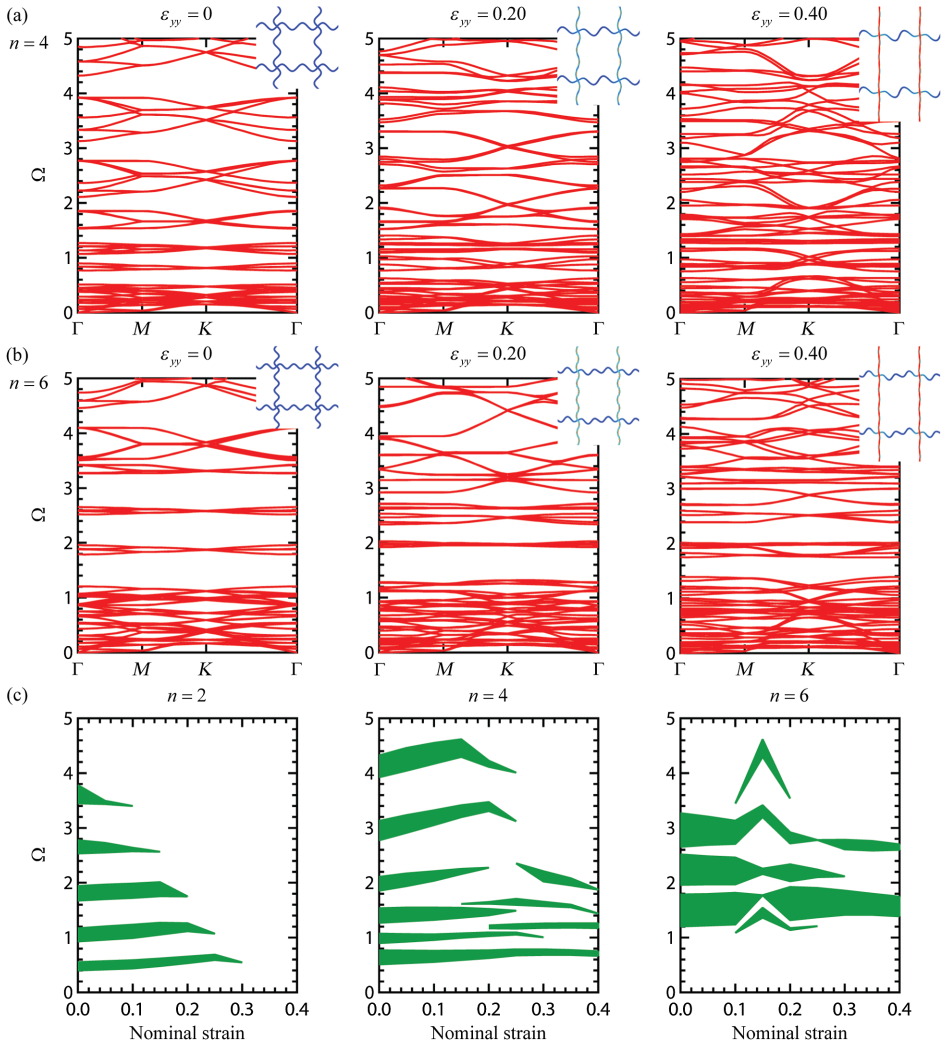

FIG. 8. Mechanically tunable band gaps for the architected lattice metamaterials. Phononic dispersion relations as a function of stretching strain for (a) $n = 4$ and (b) $n = 6$. (c) Evolution of band gaps as a function of strain for $n = 2$, $n = 4$, and $n = 6$. Here, $A_n n/l = 1/3$ and $w/l = 1/20$ for all simulations. The insets show the deformation of the unit cell at each stretching strain.

due to Bragg scattering and/or local resonances. For our lattice metamaterials, both effects can be observed in the phononic dispersion diagram. For example, for $n = 5$, local resonances are responsible for the first two band gaps, as evidenced by the flatbands between these two band gaps [Fig. 7(d)]. Other band gaps are attributed to Bragg scattering at both the microstructural level of the sinusoidally curved beam as well as the macroscopic level of lattice topology.

B. Mechanically tunable phononic band gaps

We have shown that by introducing a sinusoidal architecture into regular lattice metamaterials broad and multiple phononic band gaps can arise. It is obvious that these band gaps can be tuned by tailoring the geometric features of the ligaments (beams) of the lattice metamaterials. Here, we explore the dynamic tunability of the phononic band gaps using now an external mechanical stimulus, i.e., a uniaxial tensile deformation. Figures 8(a) and 8(b) show the phononic dispersion relations at different stretching strains for $n = 4$ and 6, respectively. We note that most of the initial band gaps will close for $n = 4$, while the band gaps tend to shrink for $n = 6$ with the increase of the applied stretching. To better understand the effect provided by the applied tensile strain we plot the evolution of the band gaps as a function of ϵ_{yy} for $n = 2, 4, 6$ [Fig. 8(c)]. It is interesting to note that for $n = 2$ all of the band gaps are suppressed when stretching the lattice material by 30%. For $n = 4$ and 6 the band gaps will partially close, while new band gaps will arise with the increase of the applied tensile strain. The sinusoidal architecture of the beams not only gives rise to broad and multiple phononic band gaps but also allows us to tune dynamically the same band gaps by virtue of the beam compliance. From a geometric perspective, this prominent vibration-control capability of the proposed lattice material is intrinsically associated with the introduced sinusoidally corrugated ligaments and its peculiar deformation behavior. These phenomena suggest that the application of a uniaxial stretching can be viewed as a useful tool to control the vibration mitigation and suppression for the proposed lattice metamaterials, which, therefore, can be used as programmable devices for wave filtering and waveguiding.

V. CONCLUSION

We have presented a class of lattice metamaterials with sinusoidally architected beams and evaluated their mechanical response and wave-propagation performance. Under uniaxial tension, the proposed sinusoidal architecture in the lattice beams provides an intrinsic deformation mechanism to switch from bending-dominated to stretching-dominated behavior. This transition of deformation mechanisms allows obtaining tunable Poisson's ratios over a large tensile strain range. Our experimental and numerical results show a very good agreement in terms of overall stress-strain relations, Poisson's ratios, and deformation patterns exhibited by these lattices. The investigation into the interplay between the multiscale (ligament and cell) architecture and wave propagation shows that broad and multiple phononic band gaps can be achieved in these lattice metamaterials. Quite importantly, this significant vibration-mitigation capability can be dynamically tuned by an external mechanical stimulus, i.e., a uniaxial stretching. Although we have not built a quantitative relation between the auxetic behavior and the vibration-mitigation capability of the lattice metamaterials, it is evident that both NPR and dynamic alleviation effects can be attributed to the unique deformation behavior and the vibrational modes of the artificially designed beams. The deformation behavior of the proposed metamaterials, together with their vibration-mitigation capability, makes them particularly suitable for the design of programmable mechanical metamaterials. The findings presented here provide insights into the development of architected metamaterials with unusual physical properties and a broad range of potential applications, such as tunable particle filters, stretchable electronics, configurable energy absorption materials, as well as adjustable acoustic metamaterials for vibration control.

ACKNOWLEDGEMENTS

The authors gratefully acknowledge the financial support from the National Science Foundation (CMMI-1437449, CMMI-1462270), the Region 2 University Transportation Research Center (UTRC), and the Office of Naval Research. Y. C. thanks Dr. Yimin (Mike) Xie, Dr. Pu Zhang (The University of Manchester), and Dr. Yongtao Sun (Tianjin University) for helpful discussion.

[1] J. H. Lee, J. P. Singer, and E. L. Thomas, Micro-/nanostructured mechanical metamaterials, Adv. Mater. **24**, 4782 (2012).

[2] J. Christensen, M. Kadic, O. Kraft, and M. Wegener, Vibrant times for mechanical metamaterials, MRS Commun. **5**, 453 (2015).

[3] T. Frenzel, C. Findeisen, M. Kadic, P. Gumbsch, and M. Wegener, Tailored buckling microlattices as reusable lightweight shock absorbers, Adv. Mater. **28**, 5865 (2016).

[4] D. R. Smith, J. B. Pendry, and M. C. Wiltshire, Metamaterials and negative refractive index, Science **305**, 788 (2004).

[5] D. R. Smith and N. Kroll, Negative Refractive Index in Left-Handed Materials, Phys. Rev. Lett. **85**, 2933 (2000).

[6] J. Valentine, S. Zhang, T. Zentgraf, E. Ulin-Avila, D. A. Genov, G. Bartal, and X. Zhang, Three-dimensional optical metamaterial with a negative refractive index, Nature (London) **455**, 376 (2008).

[7] N. Fang, D. Xi, J. Xu, M. Ambati, W. Srituravanich, C. Sun, and X. Zhang, Ultrasonic metamaterials with negative modulus, Nat. Mater. **5**, 452 (2006).

[8] H. Chen and C. Chan, Acoustic cloaking in three dimensions using acoustic metamaterials, Appl. Phys. Lett. **91**, 183518 (2007).

[9] Z. Yang, H. Dai, N. Chan, G. Ma, and P. Sheng, Acoustic metamaterial panels for sound attenuation in the 50–1000 Hz regime, Appl. Phys. Lett. **96**, 041906 (2010).

[10] Y. Chen and L. Wang, Periodic co-continuous acoustic metamaterials with overlapping locally resonant and Bragg band gaps, Appl. Phys. Lett. **105**, 191907 (2014).

[11] M. Kadic, T. Bückmann, N. Stenger, M. Thiel, and M. Wegener, On the practicability of pentamode mechanical metamaterials, Appl. Phys. Lett. **100**, 191901 (2012).

[12] B. Florijn, C. Coulais, and M. van Hecke, Programmable Mechanical Metamaterials, Phys. Rev. Lett. **113**, 175503 (2014).

[13] X. Zheng, H. Lee, T. H. Weisgraber, M. Shusteff, J. DeOtte, E. B. Duoss, J. D. Kuntz, M. M. Biener, Q. Ge, and J. A. Jackson, Ultralight, ultrastiff mechanical metamaterials, Science **344**, 1373 (2014).

[14] X. Li and H. Gao, Mechanical metamaterials: Smaller and stronger, Nat. Mater. **15**, 373 (2016).

[15] G. Wu, Y. Cho, I. S. Choi, D. Ge, J. Li, H. N. Han, T. Lubensky, and S. Yang, Directing the deformation paths of soft metamaterials with prescribed asymmetric units, Adv. Mater. **27**, 2747 (2015).

[16] S. H. Kang, S. Shan, W. L. Noorduin, M. Khan, J. Aizenberg, and K. Bertoldi, Buckling-induced reversible symmetry breaking and amplification of chirality using supported cellular structures, Adv. Mater. **25**, 3380 (2013).

[17] S. Babaee, J. Shim, J. C. Weaver, E. R. Chen, N. Patel, and K. Bertoldi, 3D Soft metamaterials with negative Poisson's ratio, Adv. Mater. **25**, 5044 (2013).

[18] H. Yasuda and J. Yang, Reentrant Origami-Based Metamaterials with Negative Poisson's Ratio and Bistability, Phys. Rev. Lett. **114**, 185502 (2015).

[19] J. N. Grima, R. Caruana-Gauci, M. R. Dudek, K. W. Wojciechowski, and R. Gatt, Smart metamaterials with tunable auxetic and other properties, Smart Mater. Struct. **22**, 084016 (2013).

[20] K. Bertoldi, P. M. Reis, S. Willshaw, and T. Mullin, Negative Poisson's ratio behavior induced by an elastic instability, Adv. Mater. **22**, 361 (2010).

[21] X. Ren, J. Shen, A. Ghaedizadeh, H. Tian, and Y. M. Xie, A simple auxetic tubular structure with tunable mechanical properties, Smart Mater. Struct. **25**, 065012 (2016).

[22] A. Ghaedizadeh, J. Shen, X. Ren, and Y. M. Xie, Tuning the performance of metallic auxetic metamaterials by using buckling and plasticity, Materials **9**, 54 (2016).

[23] D. J. Rayneau-Kirkhope and M. A. Dias, Recipes for selecting failure modes in 2-d lattices, Extreme Mech. Lett. **9**, 11 (2016).
[24] C. Coulais, Periodic cellular materials with nonlinear elastic homogenized stress-strain response at small strains, Int. J. Solids Struct. **97**, 226 (2016).
[25] M. Taylor, L. Francesconi, M. Gerendás, A. Shanian, C. Carson, and K. Bertoldi, Low porosity metallic periodic structures with negative Poisson's ratio, Adv. Mater. **26**, 2365 (2014).
[26] A. Clausen, F. Wang, J. S. Jensen, O. Sigmund, and J. A. Lewis, Topology optimized architectures with programmable Poisson's ratio over large deformations, Adv. Mater. **27**, 5523 (2015).
[27] K. E. Evans and A. Alderson, Auxetic materials: Functional materials and structures from lateral thinking!, Adv. Mater. **12**, 617 (2000).
[28] W. Yang, Z.-M. Li, W. Shi, B.-H. Xie, and M.-B. Yang, Review on auxetic materials, J. Mater. Sci. **39**, 3269 (2004).
[29] J. Grima, A. Alderson, and K. Evans, Auxetic behaviour from rotating rigid units, Phys. Status Solidi (b) **242**, 561 (2005).
[30] R. Lakes, Foam structures with a negative Poisson's ratio, Science **235**, 1038 (1987).
[31] R. Lakes, Advances in negative Poisson's ratio materials, Adv. Mater. **5**, 293 (1993).
[32] Y. Tang, G. Lin, L. Han, S. Qiu, S. Yang, and J. Yin, Design of hierarchically cut hinges for highly stretchable and reconfigurable metamaterials with enhanced strength, Adv. Mater. **27**, 7181 (2015).
[33] D. Y. Fozdar, P. Soman, J. W. Lee, L. H. Han, and S. Chen, Three-dimensional polymer constructs exhibiting a tunable negative Poisson's ratio, Adv. Funct. Mater. **21**, 2712 (2011).
[34] J. N. Grima, L. Mizzi, K. M. Azzopardi, and R. Gatt, Auxetic perforated mechanical metamaterials with randomly oriented cuts, Adv. Mater. **28**, 385 (2016).
[35] H. Mitschke, J. Schwerdtfeger, F. Schury, M. Stingl, C. Körner, R. F. Singer, V. Robins, K. Mecke, and G. E. Schröder-Turk, Finding auxetic frameworks in periodic tessellations, Adv. Mater. **23**, 2669 (2011).
[36] R. H. Baughman, J. M. Shacklette, A. A. Zakhidov, and S. Stafström, Negative Poisson's ratios as a common feature of cubic metals, Nature (London) **392**, 362 (1998).
[37] J. Grima, R. Jackson, A. Alderson, and K. Evans, Do zeolites have negative Poisson's ratios?, Adv. Mater. **12**, 1912 (2000).
[38] J. N. Grima, R. Gatt, V. Zammit, J. J. Williams, K. E. Evans, A. Alderson, and R. I. Walton, Natrolite: A zeolite with negative Poisson's ratios, J. Appl. Phys. **101**, 086102 (2007).
[39] F. Song, J. Zhou, X. Xu, Y. Xu, and Y. Bai, Effect of a Negative Poisson Ratio in the Tension of Ceramics, Phys. Rev. Lett. **100**, 245502 (2008).
[40] A. Yeganeh-Haeri, D. J. Weidner, and J. B. Parise, Elasticity of α-cristobalite: A silicon dioxide with a negative Poisson's ratio, Science **257**, 650 (1992).
[41] J.-W. Jiang and H. S. Park, Negative Poisson's ratio in single-layer graphene ribbons, Nano Lett. **16**, 2657 (2016).
[42] J. N. Grima, S. Winczewski, L. Mizzi, M. C. Grech, R. Cauchi, R. Gatt, D. Attard, K. W. Wojciechowski, and J. Rybicki, Tailoring graphene to achieve negative Poisson's ratio properties, Adv. Mater. **27**, 1455 (2015).
[43] Y. Suzuki, G. Cardone, D. Restrepo, P. D. Zavattieri, T. S. Baker, and F. A. Tezcan, Self-assembly of coherently dynamic, auxetic, two-dimensional protein crystals, Nature (London) **533**, 369 (2016).
[44] A. Slann, W. White, F. Scarpa, K. Boba, and I. Farrow, Cellular plates with auxetic rectangular perforations, Phys. Status Solidi (b) **252**, 1533 (2015).
[45] Q. Zhang, X. Xu, D. Lin, W. Chen, G. Xiong, Y. Yu, T. S. Fisher, and H. Li, Hyperbolically patterned 3D graphene metamaterial with negative Poisson's ratio and superelasticity, Adv. Mater. **28**, 2229 (2016).
[46] L. Wang and M. C. Boyce, Bioinspired structural material exhibiting post-yield lateral expansion and volumetric energy dissipation during tension, Adv. Funct. Mater. **20**, 3025 (2010).
[47] F. Javid, E. Smith-Roberge, M. C. Innes, A. Shanian, J. C. Weaver, and K. Bertoldi, Dimpled elastic sheets: A new class of non-porous negative Poisson's ratio materials, Sci. Rep. **5**, 18373 (2015).
[48] C. Lv, D. Krishnaraju, G. Konjevod, H. Yu, and H. Jiang, Origami based mechanical metamaterials, Sci. Rep. **4**, 5979 (2014).
[49] Y. Hou, R. Neville, F. Scarpa, C. Remillat, B. Gu, and M. Ruzzene, Graded conventional-auxetic Kirigami sandwich structures: Flatwise compression and edgewise loading, Composites, Part B **59**, 33 (2014).
[50] Y. Cho, J.-H. Shin, A. Costa, T. A. Kim, V. Kunin, J. Li, S. Y. Lee, S. Yang, H. N. Han, and I.-S. Choi, Engineering the shape and structure of materials by fractal cut, Proc. Natl. Acad. Sci. U.S.A. **111**, 17390 (2014).
[51] D. Prall and R. Lakes, Properties of a chiral honeycomb with a Poisson's ratio of –1, Int. J. Mech. Sci. **39**, 305 (1997).
[52] M. Bianchi, F. Scarpa, M. Banse, and C. Smith, Novel generation of auxetic open cell foams for curved and arbitrary shapes, Acta Mater. **59**, 686 (2011).
[53] L. Yang, D. Cormier, H. West, O. Harrysson, and K. Knowlson, Non-stochastic Ti–6Al–4V foam structures with negative Poisson's ratio, Mater. Sci. Eng. A **558**, 579 (2012).
[54] D. Li, L. Dong, and R. S. Lakes, The properties of copper foams with negative Poisson's ratio via resonant ultrasound spectroscopy, Phys. Status Solidi (b) **250**, 1983 (2013).
[55] Y. Li, S. Luo, M. C. Yang, R. Liang, and C. Zeng, Poisson ratio and piezoresistive sensing: A new route to high-performance 3D flexible and stretchable sensors of multimodal sensing capability, Adv. Funct. Mater. **26**, 2900 (2016).
[56] T. Widlund, S. Yang, Y.-Y. Hsu, and N. Lu, Stretchability and compliance of freestanding serpentine-shaped ribbons, Int. J. Solids Struct. **51**, 4026 (2014).
[57] Q. Ma, H. Cheng, K.-I. Jang, H. Luan, K.-C. Hwang, J. A. Rogers, Y. Huang, and Y. Zhang, A nonlinear mechanics model of bio-inspired hierarchical lattice materials consisting of horseshoe microstructures, J. Mech. Phys. Solids **90**, 179 (2016).

[58] K.-I. Jang, H. U. Chung, S. Xu, C. H. Lee, H. Luan, J. Jeong, H. Cheng, G.-T. Kim, S. Y. Han, and J. W. Lee, Soft network composite materials with deterministic and bio-inspired designs, Nat. Commun. **6**, 6566 (2015).

[59] K.-I. Jang, S. Y. Han, S. Xu, K. E. Mathewson, Y. Zhang, J.-W. Jeong, G.-T. Kim, R. C. Webb, J. W. Lee, and T. J. Dawidczyk, Rugged and breathable forms of stretchable electronics with adherent composite substrates for transcutaneous monitoring, Nat. Commun. **5**, 4779 (2014).

[60] K. Boba, M. Bianchi, G. McCombe, R. Gatt, A. C. Griffin, R. M. Richardson, F. Scarpa, I. Hamerton, and J. N. Grima, Blocked shape memory effect in negative Poisson's ratio polymer metamaterials, ACS Appl. Mater. Interfaces **8**, 20319 (2016).

[61] A. S. Phani, J. Woodhouse, and N. Fleck, Wave propagation in two-dimensional periodic lattices, J. Acoust. Soc. Am. **119**, 1995 (2006).

[62] P. Wang, F. Casadei, S. H. Kang, and K. Bertoldi, Locally resonant band gaps in periodic beam lattices by tuning connectivity, Phys. Rev. B **91**, 020103 (2015).

[63] S. Rudykh and M. C. Boyce, Transforming Wave Propagation in Layered Media via Instability-Induced Interfacial Wrinkling, Phys. Rev. Lett. **112**, 034301 (2014).

[64] See Supplemental Material at http://link.aps.org/supplemental/10.1103/PhysRevApplied.7.024012 for lattice metamaterials fabrication using 3D printing, material characterization, tensile testing, mechanical response simulation, and wave-propagation simulation.

[65] E. M. Arruda and M. C. Boyce, A three-dimensional constitutive model for the large stretch behavior of rubber elastic materials, J. Mech. Phys. Solids **41**, 389 (1993).

[66] A. S. Dalaq, D. W. Abueidda, and R. K. A. Al-Rub, Mechanical properties of 3D printed interpenetrating phase composites with novel architectured 3D solid-sheet reinforcements, Composites, Part A **84**, 266 (2016).

[67] P. Zhang and A. C. To, Transversely isotropic hyperelastic-viscoplastic model for glassy polymers with application to additive manufactured photopolymers, Int. J. Plast. **80**, 56 (2016).

[68] C. Thurnherr, L. Ruppen, G. Kress, and P. Ermanni, Nonlinear stiffness response of corrugated laminates in tensile loading, Compos. Struct. **157**, 244 (2016).

[69] L. J. Gibson and M. F. Ashby, *Cellular Solids: Structure and Properties* (Cambridge University Press, Cambridge, England, 1997).

[70] A. Khelif, Y. Achaoui, S. Benchabane, V. Laude, and B. Aoubiza, Locally resonant surface acoustic wave band gaps in a two-dimensional phononic crystal of pillars on a surface, Phys. Rev. B **81**, 214303 (2010).

[71] W. Chew and Q. Liu, Perfectly matched layers for elastodynamics: A new absorbing boundary condition, J. Comput. Acoust. **04**, 341 (1996).

[72] A. Khelif, B. Aoubiza, S. Mohammadi, A. Adibi, and V. Laude, Complete band gaps in two-dimensional phononic crystal slabs, Phys. Rev. E **74**, 046610 (2006).

[73] J. D. Achenbach, *Wave Propagation in Elastic Solids* (North-Holland, Amsterdam, 1973)

[74] M. Maldovan and E. Thomas, *Periodic Materials and Interference Lithography: For Photonics Phononics and Mechanics* (Wiley-VCH, Weinheim, 2009).

[75] G. Trainiti, J. Rimoli, and M. Ruzzene, Wave propagation in periodically undulated beams and plates, Int. J. Solids Struct. **75**, 260 (2015).